been neglected. For these compounds it has been shown that the latter "memory effects" may cancel the nearest neighbor control. Such processes have to be expected in compounds with "unstable" local electronic configurations in the absence of "memory effects".

VII. Final Outlook

The many-particle nature of π electron bonding in alternant hydrocarbon systems has been investigated by the method of the local approach supplemented by rather simple model Hamiltonians. The present authors believe that it is most convenient for the reader to review the principal findings in the form of characteristic catchwords. (i) The π electrons in annulenes and linear polyenes are sizably localized. It seems to be necessary to substitute widely accepted traditional models for π compounds. (ii) Bond alternation leads throughout to an increase in the π electron delocalization. (iii) The respective enhancement of the charge fluctuations is probably the microscopic origin for the distortive nature of π networks. (iv) An enhancement of the charge fluctuations (decreasing electronic correlation-strength Δ_i) and increasing interatomic π correlation energies caused by bond dimerization are not mutually exclusive in larger hydrocarbons. The out-of-phase modulation is obviously the rule. (v) Cyclic 6π electron structures allow for the optimum possible π delocalization in alternant hydrocarbons; but even this takes place far from the "free-electron" limit. The latter process may lead to the situation that extended π systems prefer to form more or less decoupled spatially localized 6π subunits. (vi) Extension of linear monocyclic or polycyclic π systems is frequently not coupled to an increasing delocalization of the π electrons (effects due to the end atoms neglected); their fluctuations saturate quite early. Exceptions have been discussed in the above sections. (vii) The interatomic π correlation energy is one driving force for the bond length alternation in linear and monocyclic hydrocarbons exceeding a certain threshold dimension. (viii) Strong electronic correlations tend to attenuate Jahn–Teller or Peierls instabilities. The attenuation is maximized with increasing correlation strength; see the series C_4H_4, C_8H_8, $C_{12}H_{12}$. (ix) The latter effect may be of some influence in "metastable" solids, i.e. solids where the instability is scarcely suppressed. In these compounds superconductivity under strong coupling conditions may become possible.

Acknowledgment. This work has been supported by the Deutsche Forschungsgemeinschaft and the Fonds der Chemischen Industrie. M.C.B. acknowledges support due to a Heisenberg Fellowship. The drawings have been kindly prepared by Mr. H. A. Schmaltz.

Radical Cations in Mixtures of Cl_3P and Me_2S. A Combined ESR and Quantum Chemical Study

Olav M. Aagaard,* Bas F. M. de Waal, Marcoen J. T. F. Cabbolet, and René A. J. Janssen

Laboratory of Organic Chemistry, Eindhoven University of Technology, P.O. Box 513, 5600 MB Eindhoven, The Netherlands (Received: June 10, 1991)

Exposure of phosphorus trichloride (Cl_3P) and dimethyl sulfide (Me_2S) dissolved in halocarbons ($CFCl_3$, CF_3CCl_3, $CF_2ClCFCl_2$, and CH_2Cl_2) to X rays at 77 K results in the corresponding parent cations and several cation–substrate adducts. The radicals are detected and identified by ESR spectroscopy. In dilute solution exclusive formation of the parent $Cl_3P^{\bullet+}$ and $Me_2S^{\bullet+}$ radical cations is observed. In $CFCl_3$, $Me_2S^{\bullet+}$ exhibits superhyperfine interactions due to chlorine and fluorine nuclei of the matrix molecule(s). At increased concentration, or on warming the sample, the parent radical cations readily react with dissolved Cl_3P or Me_2S molecules to form homodimeric $Cl_3P{\dot{-}}PCl_3^+$ and $Me_2S{\dot{-}}SMe_2^+$ and heterodimeric $Cl_3P{\dot{-}}SMe_2^+$ radical cations with a two-center three-electron $\sigma^2\sigma^{*1}$ bond. The heterodimer is formed in spite of a significant difference between the ionization potentials of the two constituents in reduced form. On further annealing, the $Cl_3P{\dot{-}}PCl_3^+$ cation rearranges to the well-known trigonal-bipyramidal $Cl_4P^\bullet$ radical and an as yet unidentified configuration. Candidates for the latter are proposed. In concentrated frozen solutions an unexpected reaction of $Me_2S{\dot{-}}SMe_2^+$ and Cl_3P is observed, resulting in the heterotrimer $Cl_3P(SMe_2)_2^{\bullet+}$ with an octahedral configuration, exhibiting a very large ^{31}P hyperfine interaction (A_{iso} = 5115 MHz). Extensive ab initio calculations at the HF/3-21G* level, including calculation of isotropic and dipolar electron–nuclear hyperfine interactions, confirm the assignments and provide detailed insight into the molecular geometry, electronic configuration, and stability of the radical products.

Introduction

The use of halocarbon matrices in combination with ESR spectroscopy has eminently contributed to the knowledge of radiogenic formation and reactivity of radical cations at low temperature. In general these experiments are conducted at low substrate concentration to ensure the detection of the parent radical cations and unimolecular decomposition reactions. However, at elevated concentration and depending on the temperature and mobility in the frozen halocarbon matrix, radical cations can react with free-electron pairs of other substrate molecules. Such ion–molecule reactions usually afford two-center three-electron bonds with a $\sigma^2\sigma^{*1}$ configuration (σ^* bond). Recently an increased interest has been noted in the literature on the nature and stability of these three-electron bonds. On the basis of high-level quantum chemical calculations, Clark postulates that, in vacuo, the stability of a σ^* bond will diminish exponentially with increasing difference in ionization potential of the two reduced substrates (Δ_{IP}).[1,2] Therefore, formation of an ion–molecule adduct consisting of two equivalent molecular parts (homodimer) should be preferred over ion–molecule adducts comprised of two different molecular fragments (heterodimer). Accordingly, a large number of ESR studies describe homodimeric radical cations, whereas reports on heterodimers are few. However, this reflects the lack of systematic study rather than the alledged intrinsic instability of the heterodimers.

Recently we reported the results of radiogenic radical formation in a mixture of trimethylphosphine (Me_3P) and dimethyl sulfide (Me_2S) in Freon.[3] We demonstrated that besides the well-known

---

(1) Clark, T.; Hasegawa, A.; Symons, M. C. R. *Chem. Phys. Lett.* **1985**, *116*, 79.

(2) (a) Clark, T. *J. Comput. Chem.* **1981**, *2*, 261. (b) *Ibid.* **1982**, *3*, 112. (c) *Ibid.* **1983**, *4*, 404. (d) Clark, T. *J. Am. Chem. Soc.* **1988**, *110*, 1672.

(3) Janssen, R. A. J.; Aagaard, O. M.; van der Woerd, M. J.; Buck, H. M. *Chem. Phys. Lett.* **1990**, *171*, 127.

parent radical cations ($Me_3P^{\bullet+}$ and $Me_2S^{\bullet+}$)[4,5] and homodimers ($Me_3P\dot{-}PMe_3^+$ and $Me_2S\dot{-}SMe_2^+$),[6,7] the heterodimeric ion–molecule adduct $Me_3P\dot{-}SMe_2^+$ was formed. Possibly as a result of the small Δ_{IP} (IP(Me_2S) = 8.68 eV, IP(Me_3P) = 8.60 eV, Δ_{IP} = 0.08 eV) the P$\dot{-}$S σ^* bond is intrinsically stable. In fact, detection and expected hyperfine couplings of this species had been predicted from high-level quantum chemical calculations even before experimental verification.[2,8] Nevertheless, experimental evidence also indicates that formation of a P$\dot{-}$S σ^* bond in condensed phases is hardly affected by the Δ_{IP} of the two molecular fragments involved. As an example P$\dot{-}$S σ^* bonds were also detected in X-irradiated single crystals of both trialkylphosphine sulfides ($R_3P\dot{-}S^-$),[8,9] and (methylthio)triethylphosphonium iodide ($Et_3P\dot{-}SMe$, I^-).[3] In spite of the different coordination number of the sulfur atom, which leads to strongly different ionization potentials, both radicals are readily formed and the spin-density distribution throughout these species is very similar. In a related study Abu-Raqabah and Symons very recently demonstrated that $Me_3P^{\bullet+}$ or $Ph_3P^{\bullet+}$ radical cations react at elevated temperatures with a chloride ion released by the irradiated freon solvent.[10] This results in neutral σ^* $Me_3P\dot{-}Cl$ and $Ph_3P\dot{-}Cl$ structures. Evidently, the Δ_{IP} of Me_3P and Cl^- is too large to expect a stable σ^* bond in vacuo (IP(Cl^-) = $-$EA($Cl^\bullet$) = 3.61 eV, Δ_{IP} = 4.99 eV).

The objective of the present report is to study ion–molecule reactions and adducts in mixtures of phosphorus trichloride (Cl_3P) and Me_2S in frozen halocarbon solutions. The choice for this combination was initially based on the increased Δ_{IP} (IP(Cl_3P) = 9.81 eV, Δ_{IP} = 1.13 eV) compared to the Me_3P and Me_2S combination. Our interest in the system developed during the course of this study when a variety of radical cation products and reactions was observed. Among these is the detection and identification of a radical cation composed of one Cl_3P and two Me_2S units (heterotrimer). By changing the experimental conditions, e.g. ratio or concentration of the substrates and temperature we were able to study formation and reactivity of each individual radical product. By utilizing particular freons like CF_3CCl_3 and $CF_2ClCFCl_2$, which allow for increased molecular mobility in the temperature range between 90 and 130 K,[7k,h,11] it proved possible to study ion–molecule reactions in detail. Furthermore, we use ab initio quantum chemical calculations to gain additional insight in the electronic and geometric structure of the radical cations. Both geometry optimization and hyperfine coupling calculations were performed at 3-21G* HF/SCF level. Vibrational analyses were employed to characterize the computed stationary points as local minima or saddle points.

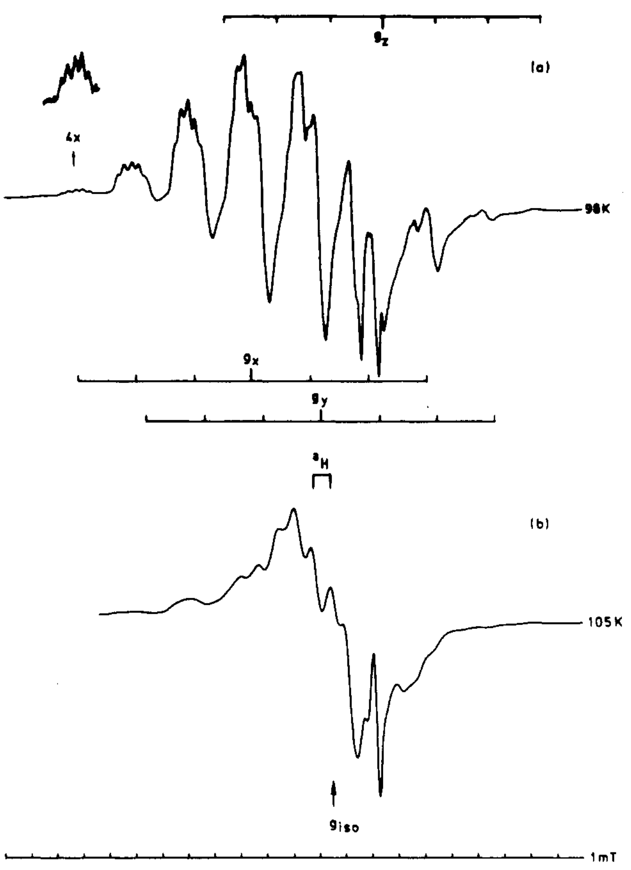

Figure 1. (a) ESR spectrum, recorded at 98 K, of the $Me_2S^{\bullet+}$ radical cation formed after X irradiation of a frozen 11% v/v Cl_3P/Me_2S (1:10) $CFCl_3$ solution. Additional ^{35}Cl and ^{19}F superhyperfine couplings appear on the g_x tensor direction. (b) ESR spectrum, recorded at 105 K, of the $Me_2S\dot{-}SMe_2^+$ radical cation formed after X irradiation of a 30% v/v Cl_3P/Me_2S (1:1) $CFCl_3$ solution.

Results and Assignment

A. Experimental. Cl_3P (Merck) was distilled prior to use. Me_2S, $CFCl_3$ (freon-11), CF_3CCl_3, and $CF_2ClCFCl_2$ (freon-113) (Aldrich) were used as received. CH_2Cl_2 (Merck) was purified over a basic-alumina column and stored on 4-Å molecular sieves. A quartz tube containing a freon or CH_2Cl_2 solution, ranging from 1 to 70% v/v Cl_3P and/or Me_2S, was degassed by repeated freeze–pump–thaw cycles in liquid nitrogen prior to irradiation and subsequently rapidly frozen at 77 K under argon. The quartz tube was transferred into a glass Dewar vessel and exposed, at 77 K, to unfiltered X irradiation from a Cu source operating at 40 kV and 20 mA for 2–6 h. The ESR spectra were recorded on a Bruker ER 200D spectrometer, operating with an X-band standard cavity and interfaced to a Bruker Aspect 3000 computer. In a typical run the field-sweep width of 0.3750 T (0.1 mT = 1 G) was sampled with 4k data points, resulting in a digital resolution of 0.09 mT (0.9 G). Expanded runs were measured with a 0.0375-T sweep width affording a 0.009-mT (0.09-G) digital resolution. The temperature was controlled with the aid of a Bruker ER 4111 variable-temperature unit. The klystron frequency was determined from ESR field positions of the hydrogen atom which is always present in X-irradiated quartz. The g values and hyperfine coupling constants, determined from the spectra, were corrected up to second order with the Breit–Rabi equations.[12] Since the powder ESR spectra can be complex due to the noncoincident g and hyperfine tensors, we expect the error in the powder assignments to be in the order of magnitude of the line width.

---

(4) $R_3\dot{P}^+$: (a) Ginns, I. S.; Mishra, S. P.; Symons, M. C. R. *J. Chem. Soc., Dalton Trans.* **1973**, 2509. (b) Fullam, B. W.; Symons, M. C. R. *J. Chem. Soc., Dalton Trans.* **1975**, 861.

(5) $R_2\dot{S}^+$: (a) Rao, D. N. R.; Symons, M. C. R.; Wren, B. W. *J. Chem. Soc., Perkin Trans. 2* **1984**, 1681. (b) Bonazzola, L.; Michaut, J. P.; Roncin, J. *J. Chem. Phys.* **1985**, *83*, 2727.

(6) P$\dot{-}$P σ^*: (a) Lyons, A. R.; Neilson, G. W.; Symons, M. C. R. *J. Chem. Soc., Chem. Commun.* **1972**, 507. (b) Lyons, A. R.; Symons, M. C. R. *J. Chem. Soc., Faraday Trans. 2* **1972**, *68*, 1589. (c) Symons, M. C. R. *Mol. Phys.* **1972**, *24*, 885. (d) Gillbro, T.; Kerr, C. M. L.; Williams, F. *Mol. Phys.* **1974**, *26*, 1225. (e) Hasegawa, A.; McConnachie, G. D. G.; Symons, M. C. R. *J. Chem. Soc., Faraday Trans. 1* **1984**, *80*, 1005. (f) Symons, M. C. R. *Chem. Soc. Rev.* **1984**, *13*, 393.

(7) S$\dot{-}$S σ^*: (a) Gilbert, B. C.; Hodgeman, D. K. C.; Norman, R. O. C. *J. Chem. Soc., Perkin Trans. 2* **1973**, 1748. (b) Gara, W. B.; Roberts, B. P. *J. Chem. Soc., Perkin Trans. 2* **1978**, 949. (d) Gara, W. B.; Giles, J. R. M.; Roberts, B. P. *J. Chem. Soc., Perkin Trans. 2* **1979**, 1444. (c) Petersen, R. L.; Nelson, D. L.; Symons, M. C. R. *J. Chem. Soc., Perkin Trans. 2* **1978**, 225. (e) Asmus, K.-D. *Acc. Chem. Res.* **1979**, *12*, 436. (f) Wang, J. T.; Williams, F. *J. Chem. Soc., Chem. Commun.* **1981**, 1184. (g) *Ibid.* **1983**, 980. (h) Qin, X.-Z.; Meng, Q.; Williams, F. *J. Am. Chem. Soc.* **1987**, *109*, 6778. (i) Illies, A. J.; Livant, P.; McKee, M. L. *J. Am. Chem. Soc.* **1988**, *110*, 7980. (j) Bonazzola, L.; Michaut, J. P.; Roncin, J. *Can. J. Chem.* **1988**, *66*, 3050. (k) Williams, F.; Qin, X.-Z. *Radiat. Phys. Chem.* **1988**, *32*, 299. (l) Anklam, E.; Asmus, K.-D. *J. Phys. Org. Chem.* **1990**, *3*, 17. (m) Ambroż, H. B.; Przybytniak, G. K.; Wrońska, T. *Radiat. Phys. Chem.* **1991**, *37*, 479.

(8) Janssen, R. A. J.; Kingma, J. A. J. M.; Buck, H. M. *J. Am. Chem. Soc.* **1988**, *110*, 3018.

(9) Aagaard, O. M.; Janssen, R. A. J.; Buck, H. M. *Rec. Trav. Chim. Pays-Bas* **1989**, *108*, 262.

(10) (a) Abu-Raqabah, A.; Symons, M. C. R. *J. Chem. Soc., Faraday Trans.* **1990**, *86*, 3293. (b) *Ibid. J. Am. Chem. Soc.* **1990**, *112*, 3293.

(11) Sjoqvist, L.; Lindgren, M.; Lund, A. *Chem. Phys. Lett.* **1989**, *156*, 323.

(12) Breit, G.; Rabi, I. I. *Phys. Rev.* **1931**, *38*, 2082.

(13) Wang, J. T.; Williams, F. *J. Am. Chem. Soc.* **1981**, *103*, 6994.

TABLE I: ^{1}H Hyperfine Couplings[a] and g Values of the $Me_2S^{\bullet+}$ Radical Cation, Its Homodimer $Me_2S—\dot{}SMe_2^+$ and Related Radical Cations Generated in Irradiated Halocarbon Solutions

radical	T, K	A, MHz	g_x	g_y	g_z	g_{iso}
$Me_2O^{\bullet+}$	77[b]	123; 119; 119	2.0138	2.0072	2.0045	2.0085
$Me_2S^{\bullet+}$	81[c]	57	2.019	2.019	2.0023	2.0134
	124[d]	57	2.019	2.0145	2.0076	2.0137
	77[e]	61; 60; 57	2.033	2.016	2.001	2.017
	77[f]		2.032		2.002	2.012
	130[f]	59	2.019	2.0145	2.0076	2.0137
	98[g]	60; 60; 56	2.032	2.015	2.001	2.016
	77[h]	58; 58; 56	2.033	2.017	2.002	2.017
	81[i]	58	2.032	2.017	2.002	2.017
$Me_2S\overset{\bullet}{—}SMe_2^+$	120[c]	18				2.010
	158[j]	18				2.0102
	295[k]	19				2.0103
	100[i]	18				2.010
	105[g]	19				2.012
$Me_2Se^{\bullet+}$	77[l]	44	2.1316	2.0647	1.999	2.0651
$Me_2Se\overset{\bullet}{—}SeMe_2^+$	77[m]	13	2.0702	2.0366	1.9964	2.0344

[a] $A_i(\text{MHz}) = 2.80247\,(g_i/g_e)\,a_i(\text{G})$. [b] $CFCl_3$, ref 13. [c] CF_3CCl_3, ref 7h. [d] $CFCl_3$, refs 7f,g. [e] $CFCl_3$, ref 5b. [f] $CFCl_3$, ref 5a. [g] $CFCl_3$, this study. [h] $CF_2ClCFCl_2$, ref 5b. [i] $CF_2ClCFCl_2$, ref 7k. [j] Cyclopropane, ref 7d. [k] H_2O, ref 7a. [l] $CFCl_3$, ref 1. [m] Single crystal of Me_2Se, ref 21.

The $Me_2S^{\bullet+}$ and $Me_2S\dot{-}SMe_2^+$ Radical Cations. ESR studies on both radicals are numerous.[5,7] Table I lists some interesting literature data along with the results of the present study. The $Me_2S^{\bullet+}$ and $Me_2S\dot{-}SMe_2^+$ radical cations can be distinguished by the larger ^{1}H hyperfine coupling of the $Me_2S^{\bullet+}$ radical cation (60 vs 18 MHz, Figure 1). Furthermore, the g tensor of $Me_2S^{\bullet+}$ is strongly anisotropic whereas the g value of $Me_2S\dot{-}SMe_2^+$ seems isotropic (Figure 1). In Figure 1a the ESR spectrum of the $Me_2S^{\bullet+}$ radical cation in $CFCl_3$ at 98 K nicely illustrates the complex pattern caused by the overlapping ^{1}H hyperfine couplings and the anisotropic g tensor of the radical. Our assignment, indicated in Figure 1a, corresponds well with g values reported by Bonazzola et al.[5b] Prior to annealing, the spectrum at low temperature clearly exhibits additional hyperfine couplings on the g_x direction. These splittings have been attributed by Rao et al.[5a] to weak σ^* bonding between $Me_2S^{\bullet+}$ and a chlorine atom of $CFCl_3$. A closer look, however, reveals a five-line pattern (ratio 1:2:2:2:1) pointing to more nuclei contributing to the superhyperfine interaction. The pattern can be interpreted by a 7.0-MHz (2.5-G) superhyperfine interaction of one ^{35}Cl and one ^{19}F nucleus. Likewise, extra hyperfine splittings of 4.2 MHz (1.5 G) were resolved on the g_z component, though no explicit pattern could be established. In agreement with previous studies, no extra coupling was resolved on the g_y tensor component. In this respect, however, it is interesting to note that Rao et al.[5a] reported an extra 4.2-MHz (1.5-G) splitting on the g_y direction of the $(CD_3)_2S^{\bullet+}$ radical cation, which was well resolved as a result of an integer ratio of the ^{2}H (8.4 MHz, 3.0 G) and ^{35}Cl (4.2 MHz, 1.5 G) couplings. Weak matrix interactions of radical cations to either ^{35}Cl or ^{19}F are frequently observed in $CFCl_3$ solutions,[1,5a,14] but we believe that $Me_2S^{\bullet+}$ is the first example where ^{35}Cl and ^{19}F interactions are observed simultaneously.

With respect to formation and stability of these cations we find that X irradiation of a mixture of Me_2S and Cl_3P invariably leads to $Me_2S^{\bullet+}$ at low Me_2S concentration, and to $Me_2S\dot{-}SMe_2^+$ dimers at increased concentration. It is interesting to note that, in contrast to their concurrent detection in the mobile CF_3CCl_3 and $CF_2ClCFCl_2$ matrices, we were not able to observe the monomer and dimer radical cations simultaneously in the more rigid $CFCl_3$ or CH_2Cl_2 matrices. In $CFCl_3$, e.g., formation of either the monomer or dimer radical cation is determined by the Me_2S concentration. If the concentration is below 10% v/v, only $Me_2S^{\bullet+}$ is observed; above 10% v/v, solely the $Me_2S\dot{-}SMe_2^+$ radical cation is detected. A similar behavior was recently noted by Ambrož et al.[7m] In $CFCl_3$ the monomeric radical cation can be detected until the melting of the $CFCl_3$ matrix (145 K). The dimer cation is stable up to 135 K at which temperature the signal intensity rapidly decreases.

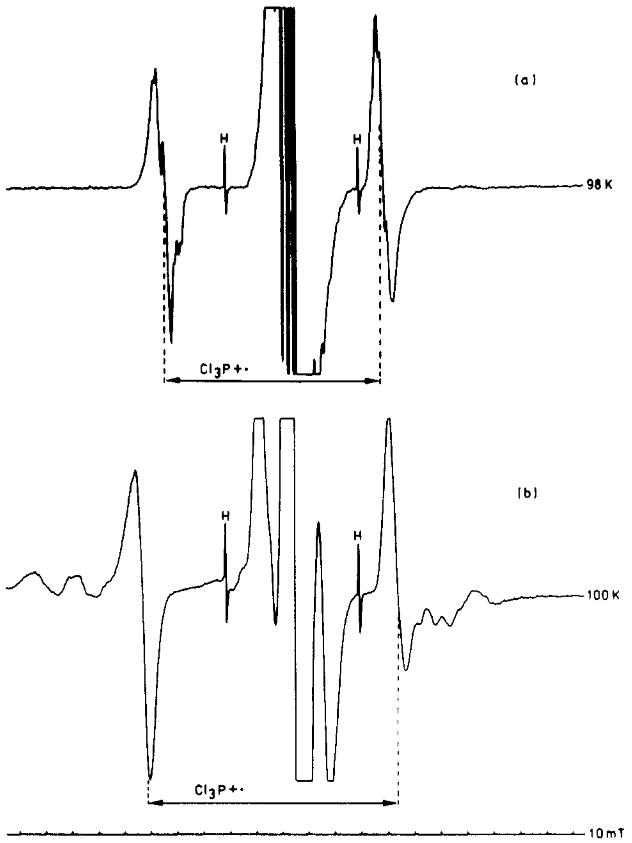

Figure 2. (a) ESR spectrum recorded at 98 K of the $Cl_3P^{\bullet+}$ radical cation formed radiogenically in a 11% v/v Cl_3P/Me_2S (1:10) $CFCl_3$ solution. Additional ^{35}Cl hyperfine interactions are present. (b) ESR spectrum of the $Cl_3P^{\bullet+}$ radical cation formed in a 10% v/v solution of Cl_3P in CH_2Cl_2.

The $Cl_3P^{\bullet+}$ Radical Cation. X irradiation of Cl_3P results in the formation of the corresponding $Cl_3P^{\bullet+}$ radical cation in all halocarbons used. The ESR spectrum of this radical generated in $CFCl_3$ is depicted in Figure 2a. The spectrum reveals a large, nearly isotropic, ^{31}P doublet with some partially resolved chlorine hyperfine splittings. The isotropic ^{31}P coupling derived from this spectrum is in agreement with values established for the related $(HO)_3P^{\bullet+}$ and $(MeO)_3P^{\bullet+}$ radical cations.[4,6e,f] Interestingly, the ESR spectrum of the $Cl_3P^{\bullet+}$ radical cation generated from Cl_3P

---

(14) (a) Eastland, G. W.; Rao, D. N. R.; Rideout, J.; Symons, M. C. R.; Hasegawa, A. *J. Chem. Res.* (*S*) **1983**, 258. (b) Eastland, G. W.; Maj, S. P.; Symons, M. C. R.; Hasegawa, A.; Glidewell, C.; Hayashi, M.; Wakabayashi, T. *J. Chem. Soc., Perkin Trans. 2* **1984**, 1439. (c) McConnachie, G. D. C.; Symons, M. C. R. *J. Chem. Res.* (*S*) **1985**, 54.

TABLE II: Hyperfine Couplings[a] and *g* Values of the Radicals Detected in X-Irradiated Mixtures of Cl_3P and Me_2S, and Related Radical Structures Reported in the Literature

radical	T, K	A_x, MHz x	^{31}P	^{35}Cl	g_x
$Cl_2P^\bullet$	75[b]	$\parallel$	739	40	2.001
		$\perp_1$	−95	−14	2.023
		$\perp_2$	−75	−21	2.014
		iso	190	2	2.013
		2dip	549	38	
$Cl_4P^\bullet$	77[c]	$\parallel$	3553	178	2.00
		$\perp$	3391	56	2.02
		iso	3445	96	2.02
		2dip	108	82	
	130[d,e]	iso	3638		2.024
"X"	130[d,e]	iso	3945		2.022
$Cl_3P^{\bullet+}$	98[d,f]	iso	2330	65	2.025
	98[e]	iso	2682		2.025
$(HO)_3P^{\bullet+}$	77[g]	$\parallel$	2605		
		$\perp$	2039		
		iso	2227		
		2dip	378		
$(MeO)_3P^{\bullet+}$	77[h]	$\parallel$	2524		2.0038
		$\perp$	1998		2.0026
		iso	2173		2.003
		2dip	351		
	77[i]	$\parallel$	2812		2.0049
		$\perp$	2255		2.004
		iso	2441		2.0043
		2dip	371		
$Me_3P^{\bullet+}$	100[j]	$\parallel$	1636		2.002
		$\perp$	813		2.007
		iso	1087		2.005
		2dip	549		

[a] $A_i(\mathrm{MHz}) = 2.80247(g_i/g_e)\ a_i(\mathrm{G})$. [b] Single crystal of Cl_3P, ref 15i. [c] Frozen Cl_3P, refs 15c,h. [d] $CFCl_3$, this study. [e] CH_2Cl_2, this study. [f] CF_3CCl_3 and $CF_2ClCFCl_2$, this study. [g] H_3PO_4 in H_2SO_4, ref 4a. [h] $CFCl_3$, refs 6e,f. [i] CCl_4, refs 6e,f. [j] $CFCl_3$, ref 3.

in a CH_2Cl_2 matrix (Figure 2b) exhibits a ^{31}P hyperfine interaction which is substantially larger (Table II), whereas no chlorine hyperfine interactions are resolved. A similar difference in hyperfine coupling constants and appearance of the spectrum has previously been reported by Symons and co-workers for the $(MeO)_3P^{\bullet+}$ radical cation in $CFCl_3$ and CCl_4 matrices.[6e,f] They suggested that the $(MeO)_3P^{\bullet+}$ radical cation can adopt two different conformations: a spherical structure (C_3) in CCl_4 and an oblate structure (C_s) in $CFCl_3$. In case of $Cl_3P^{\bullet+}$, different radical conformations are less obvious, and differences, when of an intramolecular nature, can only be rationalized by a change of hybridization of the central phosphorus atom, e.g. flattening of the radical structure (in extreme C_{3v} to D_{3h}). On the other hand, a specific electronic interaction with the matrix molecules cannot be ruled out.

The $Cl_3P^{\bullet+}$ radical cation is relatively stable in all halocarbon matrices up to high concentration of Cl_3P (20% v/v, Table II). However, it is absent if the cosolute Me_2S is present at a concentration over 10% v/v.

The $Cl_4P^\bullet$ Radical. The $Cl_4P^\bullet$ radical is readily detected after X irradiation of Cl_3P in a CH_2Cl_2 matrix. It is well-known that $Cl_4P^\bullet$ possesses a trigonal-bipyramidal type structure in which the odd electron is located in a vacant equatorial position (TBP-e). The ^{31}P hyperfine interaction (Table II) is in good accordance with literature values for this radical generated in pure Cl_3P.[15]

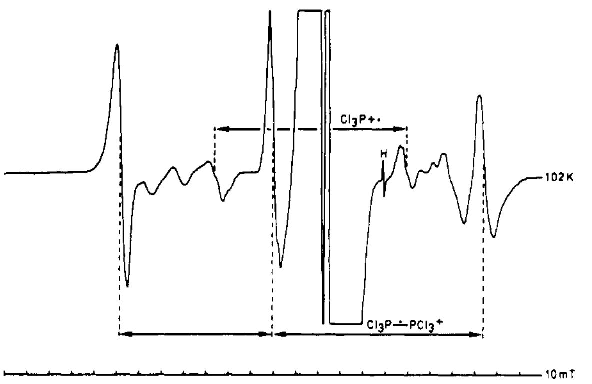

Figure 3. ESR spectrum, recorded at 102 K, of the $Cl_3P\dot{-}PCl_3^+$ radical cation formed in a 10% v/v solution of Cl_3P in $CFCl_3$.

TABLE III: ^{31}P Hyperfine Couplings[a] and *g* Values of Homo- and Heterodimeric Radical Cations Detected in X-Irradiated Mixtures of Cl_3P and Me_2S, and Related Radical Structures Reported in the Literature

radical	T, K	x	A_x, MHz	g_x
$Cl_3P\dot{-}PCl_3^+$	102[b]	iso	2260	2.020
$Me_3P\dot{-}PMe_3^+$	100[c]	$\parallel$	1605	1.998
		$\perp$	1333	2.006
		iso	1424	2.003
		2dip	181	
$Cl_3P\dot{-}SMe_2^+$	100[d]	iso	3360	2.016
$Me_3P\dot{-}SMe_2^+$	100[c]	$\parallel$	1840	2.003
		$\perp$	1385	2.006
		iso	1537	2.005
		2dip	303	
$Cl_5P^{\bullet-}$	77[e]	$\parallel$	4619	2.00
		$\perp$	4523	2.02
		iso	4555	2.02
		2dip	64	
$Cl_3P(SMe_2)_2^{\bullet+}$	120[d,f]	iso	5115	2.023

[a] $A_i(\mathrm{MHz}) = 2.80247(g_i/g_e)\ a_i(\mathrm{G})$. [b] $CFCl_3$, and CH_2Cl_2, this study. [c] $CFCl_3$, ref 3. [d] $CFCl_3$, CH_2Cl_2, and $CF_2ClCFCl_2$, this study. [e] Cl_5P, ref 15h. [f] CF_3CCl_3, this study.

In the present case no chlorine hyperfine couplings were resolved. When generated in a $CFCl_3$ matrix, the ESR absorptions of $Cl_4P^\bullet$ increase upon annealing. In this case $Cl_4P^\bullet$ seems to be a secondary radical product because the rise of signal intensity coincides with the gradual loss of the $Cl_3P\dot{-}PCl_3^+$ radical (vide infra). The $Cl_4P^\bullet$ radical was not observed in CF_3CCl_3 and $CF_2ClCFCl_2$ matrices.

The $Cl_3P\dot{-}PCl_3^+$ Radical Cation. X irradiation of Cl_3P in $CFCl_3$ or CH_2Cl_2 at relatively low concentration (>3% v/v) results in the formation of the homodimeric $Cl_3P\dot{-}PCl_3^+$ radical cation from an ion–molecule reaction of $Cl_3P^{\bullet+}$ with Cl_3P. The presence of $Cl_3P\dot{-}PCl_3^+$ cations is readily recognized by the degenerate triplet ESR spectrum shown in Figure 3, which is characteristic for a $P\dot{-}P$ σ^* type radical. As a result of the large hyperfine interaction to two identical ^{31}P nuclei, the spectrum consists of four equally intense absorptions caused by a second-order splitting of the original degenerate central lines. In fact only three of the four lines can be identified because the fourth absorption is obscured by a strong central signal from the irradiated quartz tube. The ^{31}P hyperfine coupling is listed in Table III. No ^{35}Cl or ^{37}Cl hyperfine interactions were resolved. Upon annealing, the radical can be detected up to 130–135 K. The decay of the radical cation seems to be coupled with the increase of the TBP-e $Cl_4P^\bullet$ radical and another, as yet unidentified, phosphorus-centered radical (vide infra). In contrast to the parent radical cation $Cl_3P^{\bullet+}$, the magnitude of the ^{31}P hyperfine interaction is identical in $CFCl_3$ and CH_2Cl_2. Surprisingly, the $Cl_3P\dot{-}PCl_3^+$ radical cation is not observed after X irradiation of Cl_3P in the mobile CF_3CCl_3 and $CF_2ClCFCl_2$ matrices.

The $Cl_3P\dot{-}SMe_2^+$ Radical Cation. The $Cl_3P\dot{-}SMe_2^+$ radical

---

[15] $Cl_2P^\bullet$ and $Cl_4P^\bullet$: (a) Kokoszka, G. F.; Brinckman, F. E. *J. Chem. Soc., Chem. Commun.* **1968**, 349. (b) Kokoszka, G. F.; Brinckman, F. E. *J. Am. Chem. Soc.* **1971**, *92*, 1199. (c) Begum, A.; Symons, M. C. R. *J. Chem. Soc. A* **1971**, 2065. (d) Kerr, C. M. L.; Williams, F. *J. Phys. Chem.* **1971**, *75*, 3023. (e) Wei, M. S.; Current, J. H.; Gendell, J. *J. Chem. Phys.* **1972**, *57*, 2431. (f) Fullam, B. W.; Mishra, S. P.; Symons, M. C. R. *J. Chem. Soc., Dalton Trans.* **1974**, 2145. (g) Kerr, C. M. L.; Webster, K.; Williams, F. *J. Phys. Chem.* **1975**, *79*, 2663. (h) Mishra, S. P.; Symons, M. C. R. *J. Chem. Soc., Dalton Trans.* **1976**, 139. (i) Bonazzola, L.; Michaut, J. P.; Roncin, J. *J. Chem. Phys.* **1981**, *75*, 4829.

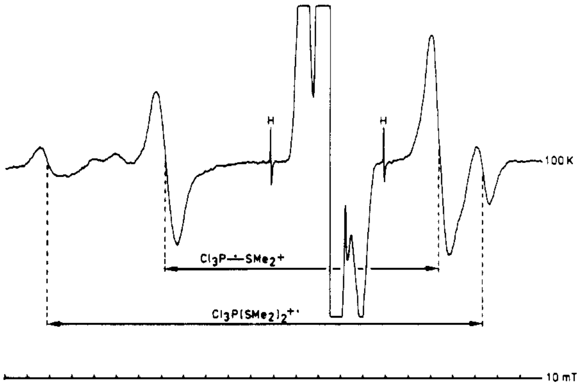

Figure 4. ESR spectrum, recorded at 100 K, of the heterodimer $\mathrm{Cl_3P\dot{-}SMe_2^+}$ radical cation formed in a 70% v/v solution of $\mathrm{Cl_3P}$ and $\mathrm{Me_2S}$ (1:1) in $\mathrm{CFCl_3}$.

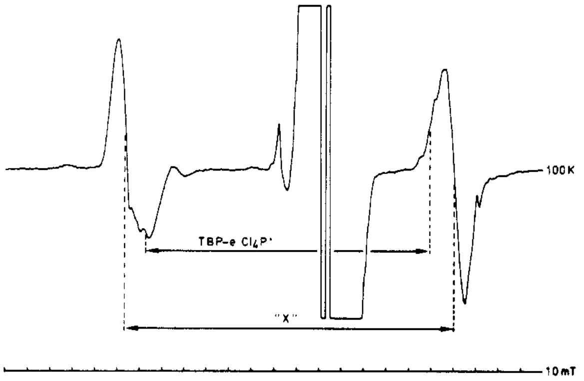

Figure 5. ESR spectrum, recorded at 100 K, of the $\mathrm{Cl_4P^\bullet}$ and "X" radicals formed from $\mathrm{Cl_3P\dot{-}PCl_3^+}$ after short annealing the sample to 148 K. The spectrum was obtained after X irradiation of a 10% v/v solution of $\mathrm{Cl_3P}$ in $\mathrm{CFCl_3}$.

cation is readily produced when both $\mathrm{Me_2S}$ and $\mathrm{Cl_3P}$ are present in concentrations above 3% in spite of the nonzero Δ_{IP} of the two molecular fragments involved. The ^{31}P hyperfine coupling (Table III) derived from the ESR spectrum shown in Figure 4 exhibits the expected increase with respect to the $\mathrm{Cl_3P^{\bullet+}}$ and $\mathrm{Me_3P\dot{-}SMe_2^+}$ radical cations. There is little doubt that the spectrum corresponds to the $\mathrm{Cl_3P\dot{-}SMe_2^+}$ heterodimer radical cation. Analogous to radiogenic formation of $\mathrm{Me_3P\dot{-}SMe_2^+}$ in $\mathrm{CFCl_3}$ matrices,[3] the structure of $\mathrm{Cl_3P\dot{-}SMe_2^+}$ is assigned to a $\mathrm{P\dot{-}S}$ σ^* type radical. Evidently, formation of $\mathrm{Cl_3P\dot{-}SMe_2^+}$ can be rationalized by two different reaction pathways: $\mathrm{Cl_3P^{\bullet+} + Me_2S \rightarrow Cl_3P\dot{-}SMe_2^+ \leftarrow Cl_3P + Me_2S^{\bullet+}}$. It is experimentally not possible to distinguish between these alternatives. In $\mathrm{CFCl_3}$, slight warming results in the irreversible loss of the radical at 120 K. This might be interpreted as an intrinsically lower stability of the heterodimer compared to the homodimers $\mathrm{Me_2S\dot{-}SMe_2^+}$ and $\mathrm{Cl_3P\dot{-}PCl_3^+}$. No other radicals are detected on further annealing.

The "X" Radical. Upon annealing an X-irradiated sample of 10% v/v $\mathrm{Cl_3P}$ in $\mathrm{CFCl_3}$, we clearly detected a transition of $\mathrm{Cl_3P\dot{-}PCl_3^+}$ into the TBP-e $\mathrm{Cl_4P^\bullet}$ radical and a second unidentified phosphorus-centered radical (hereby called "X"). The rearrangement is also noted in $\mathrm{CH_2Cl_2}$ but not in $\mathrm{CF_3CCl_3}$ or $\mathrm{CF_2ClCFCl_2}$ (Table III). The corresponding ESR spectrum is shown in Figure 5. Both the TBP-e $\mathrm{Cl_4P^\bullet}$ and "X" radicals are stable up to the melting of the matrix. The radicals are formed when $\mathrm{Cl_3P}$ is X irradiated without $\mathrm{Me_2S}$ as cosolute. Evidently, they are derived from $\mathrm{Cl_3P}$ alone, and a relatively low concentration of the parent substrate is sufficient (>3%). The magnitude of the ^{31}P hyperfine coupling of "X" (Table II) indicates that the structure is similar to the TBP-e $\mathrm{Cl_4P^\bullet}$ radical. Essentially two candidates can be proposed for "X". First it can be assigned to a $\mathrm{Cl_4P^\bullet}$ trigonal-bipyramidal structure in which the odd electron occupies the vacant axial location (TBP-a). Ab initio quantum chemical calculations on C_{2v} (TBP-e) and C_{3v} (TBP-a) $\mathrm{H_4P^\bullet}$ and $\mathrm{F_4P^\bullet}$ radicals[16] predict that the TBP-a structure should exhibit a larger ^{31}P hyperfine coupling than the TBP-e configuration. This would agree nicely with the present experiment (Figure 5, Table II). The second candidate is a σ^* $\mathrm{Cl_3P\dot{-}Cl}$ radical structure. Abu-Raqabah and Symons reported formation of similar σ^* $\mathrm{R_3P\dot{-}Cl}$ radicals by reaction of a $\mathrm{R_3P^{\bullet+}}$ radical cation and a chloride ion descendent from the irradiated solvent.[10] However, at this moment no clear assignment can be made, and it is also conceivable that radical "X" does not correspond to either of the suggested structures.

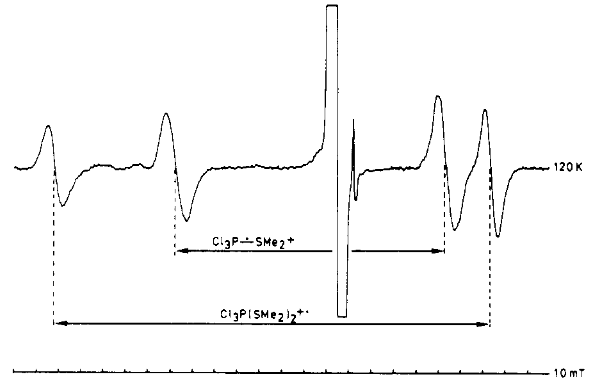

Figure 6. ESR spectrum, recorded at 120 K, of the heterotrimer $\mathrm{Cl_3P(SMe_2)_2^{\bullet+}}$ radical cation formed by ion-molecule reaction of $\mathrm{Me_2S\dot{-}SMe_2^+}$ and $\mathrm{Cl_3P}$. The radicals are generated in a 70% v/v solution of $\mathrm{Cl_3P}$ and $\mathrm{Me_2S}$ (1:1) in $\mathrm{CFCl_3}$.

The $\mathrm{Cl_3P(SMe_2)_2^{\bullet+}}$ Radical Cation. Upon annealing an X-irradiated frozen mixture of $\mathrm{Cl_3P}$ and $\mathrm{Me_2S}$ (for instance 70% v/v 1:1 in $\mathrm{CFCl_3}$) a new phosphorus-centered radical is formed, exhibiting a very large ^{31}P hyperfine coupling of 5115 MHz (Figure 6, Table III). The magnitude of the isotropic ^{31}P hyperfine coupling points to a high contribution of the phosphorus 3s orbital to the SOMO.[17] To our knowledge, the largest ^{31}P hyperfine coupling reported until now amounts to 4555 MHz attributed to the $\mathrm{Cl_5P^{\bullet-}}$ radical anion which possesses an octahedral structure with the unpaired electron in a vacant position.[15b] This suggests that in our case the central phosphorus atom bears at least five substituents. We assign the new formed radical to the $\mathrm{Cl_3P(SMe_2)_2^{\bullet+}}$ radical cation formed by reaction of $\mathrm{Me_2S\dot{-}SMe_2^+}$ with a $\mathrm{Cl_3P}$ molecule. Our assignment is based on several observations. First, the larger ^{31}P hyperfine coupling of $\mathrm{Cl_3P(SMe_2)_2^{\bullet+}}$ compared to $\mathrm{Cl_5P^{\bullet-}}$ can be explained by the fact that the positively charged $\mathrm{SMe_2}$ substituents accommodate the valence electrons better than the chlorine atoms of $\mathrm{Cl_5P^{\bullet-}}$, thereby increasing spin density on the hypervalent phosphorus nucleus in the antibonding SOMO. Second, the $\mathrm{Cl_3P(SMe_2)_2^{\bullet+}}$ radical is only detected when both $\mathrm{Me_2S}$ and $\mathrm{Cl_3P}$ are present, which points to a hetero ion-molecule reaction. Furthermore, the increase of the $\mathrm{Cl_3P(SMe_2)_2^{\bullet+}}$ concentration is coupled with a rapid decrease of the $\mathrm{Me_2S\dot{-}SMe_2^+}$. In $\mathrm{CFCl_3}$, the radical is absent if the concentration of $\mathrm{Me_2S}$ is below 10% v/v, regardless of the $\mathrm{Cl_3P}$ concentration (only formation of $\mathrm{Me_2S^{\bullet+}}$!). In addition, the radical is formed in $\mathrm{CF_3CCl_3}$ although the heterodimer $\mathrm{Cl_3P\dot{-}SMe_2^+}$ is not observed. This signifies that the ion-molecule reaction between the heterodimer $\mathrm{Cl_3P\dot{-}SMe_2^+}$ and a molecule of $\mathrm{Me_2S}$ is unlikely. Apparently, the $\mathrm{Me_2S\dot{-}SMe_2^+}$ radical cation reacts with a $\mathrm{Cl_3P}$ molecule giving the *trimer* radical cation. Formation of this radical is observed in all halocarbon matrices used. The trimer vanishes before the matrices melt without generating new phosphorus-centered radicals.

It is noted that Illies et al.[7i] report a similar reaction. In a mass spectroscopic study on the homoassociation of $\mathrm{Me_2S^{\bullet+}}$ to $\mathrm{Me_2S}$, they observed at −40 °C a prominent peak at m/z 182. It is assigned to the monopositive trimer of $\mathrm{Me_2S}$ *less four amu.*

---

(16) (a) Howell, J. M.; Olsen, J. F. *J. Am. Chem. Soc.* **1976**, *98*, 7119. (b) Janssen, R. A. J.; Visser, G. J.; Buck, H. M. *J. Am. Chem. Soc.* **1984**, *106*, 3429. (c) Janssen, R. A. J.; Buck, H. M. *J. Mol. Struc.* (*THEOCHEM*) **1984**, *110*, 139. (d) Cramer, C. J. *J. Am. Chem. Soc.* **1991**, *113*, 2439.

(17) Morton, J. R.; Preston, K. F. *J. Magn. Reson.* **1978**, *30*, 577.

TABLE IV: Total Energies (au)[a] and $\langle S^2\rangle_{UHF}$ Expectation Values of the Radical Precursors and Radicals at Their Equilibrium Geometries (Figures 7–11) (All Structures Were Calculated with the 3-21G* Basis Set)

compound	symmetry	UHF	ROHF	RHF	$\langle S^2\rangle$
$H_2S^{\bullet+}$	C_{2v}	−396.476 386	−396.471 563		0.7611
H_2S	C_{2v}			−396.819 637	
$H_2S\overset{\bullet}{-}SH_2^+$	C_{2h}	−793.332 709	−793.325 431		0.7717
$Me_2S^{\bullet+}$	C_{2v}	−474.174 441	−474.169 419		0.7628
Me_2S	C_{2v}			−474.456 985	
$Me_2S\overset{\bullet}{-}SMe_2^+$	C_{2h}	−948.663 185	−948.656 055		0.7734
Cl_2P^+	C_{2v}			−1253.595 142	
$Cl_2P^\bullet$	C_{2v}	−1253.922 205	−1253.917 335		0.7671
$Cl_3P^{\bullet+}$	C_{3v}	−1711.015 964	−1711.012 755		0.7606
Cl_3P	C_{3v}			−1711.356 885	
$Cl_4P^\bullet$	C_{2v}	−2168.721 431	−2168.714 223		0.7874
	$C_{3v}{}^b$	−2168.710 450	−2168.703 551		0.7882
$Cl_5P^{\bullet-}$	C_{4v}	−2626.219 457	−2626.213 718		0.7815
$Cl_3P\overset{\bullet}{-}SH_2^+$	C_s	−2107.859 525	−2107.853 847		0.7714
$Cl_3PPCl_3^{\bullet+}$	C_{2h}	−3422.387 232	−3422.380 975		0.7804
	C_{2v}	−3422.321 490	*e*		0.7893
	C_s	−3422.382 358	*e*		0.7609
$Cl_3P(SH_2)_2^{\bullet+}$	$C_{2v}(1)^c$	−2504.652 301	−2504.644 628		0.7928
	C_2	−2504.652 200	*e*		0.7942
	$C_{2v}(2)$	−2504.651 054	*e*		0.7936
	$C_s{}^d$	−2504.683 459	*e*		0.7609

[a] 1 au = 627.5 kcal/mol. [b] Degenerate imaginary frequency 118*i* cm^{-1}, E. [c] Imaginary frequencies 92*i* cm^{-1}, B_2; 52*i* cm^{-1}, B_1. [d] Imaginary frequencies 89*i* cm^{-1} and 29*i* cm^{-1}, A″. [e] No SCF convergence.

However, as they state: "the structure of this species is a tantalizing mystery".[7i]

B. Quantum Chemical Calculations. All calculations employed the GAUSSIAN88[18] or GAMESS UK[19] series of programs using the 3-21G* basis set. Odd-electron systems were calculated using the unrestricted and restricted open-shell Hartree–Fock (UHF and ROHF) formalisms, and closed-shell systems with restricted Hartree–Fock (RHF). For open-shell systems geometry optimization was started at the UHF level. The resulting structure then served as input to the ROHF geometry optimization. Harmonic vibrational frequencies were calculated at the 3-21G* level in order to characterize stationary points as minima (representing equilibrium structures) or saddle points (transition states). Magnetic properties such as the isotropic and anisotropic part of the electron–nuclear hyperfine interaction were determined, where possible, from the spin-density matrix. The isotropic hyperfine coupling was calculated from

$$A_{iso} = {}^8/_3\pi g_e\beta_e g_N\beta_N|\psi_N(0)|^2 \qquad (1)$$

with

$$|\psi_N(0)|^2 = \sum_{\mu\nu} P^{\alpha-\beta}_{\mu\nu}\langle\phi_\mu|\delta(r_N)|\phi_\nu\rangle \qquad (2)$$

being the Fermi contact integral, and in which $P^{\alpha-\beta}_{\mu\nu}$ is the spin-density matrix. It is noted that the GAMESS UK program package gives the Fermi contact integral $^1/_2\pi$ times its true value (in au). The magnetic dipolar hyperfine tensor was calculated as

$$A_{dip}(u,v) = -g_e\beta_e g_N\beta_N\sum_{\mu\nu}P^{\alpha-\beta}_{\mu\nu}\left\langle\phi_\mu\left|\frac{(r^2\delta_{uv} - 3uv)}{r^5}\right|\phi_\nu\right\rangle \qquad (3)$$

where u, v are the Cartesian coordinates x, y, z. Subsequent diagonalization of the matrix results in the three principal values of A_{dip} and the corresponding direction cosines. Optimized geometries are given in Figures 7–11 and their total energies are listed in Table IV.

TABLE V: Calculated Isotropic and Anisotropic Hyperfine Couplings (MHz) of Nuclei with Sufficient Spin Density in the Calculated Radical Structures Using the ROHF Wave Function[a] (Figures 7–11)

radical	symmetry	nucleus	A_{iso}	A_{dip} 1	A_{dip} 2	A_{dip} 3
$H_2S^{\bullet+}$	C_{2v}	H	0	−21	−2	23
$H_2S\overset{\bullet}{-}SH_2^+$	C_{2h}	H	0	−12	0	12
$Me_2S^{\bullet+}$	C_{2v}	H_{avg}	20	−5	−4	9
$Me_2S\overset{\bullet}{-}SMe_2^+$	C_{2h}	H_{avg}	8	−5	−3	8
$Cl_3P^{\bullet+}$	C_{3v}	P	1459	−196	−196	392
		Cl	8	−17	−17	34
$Cl_4P^\bullet$	C_{2v}	P	2151	−98	−98	196
		Cl_1	36	−34	−34	68
		Cl_2	3	−3	−3	6
	C_{3v}	P	2537	−87	−87	174
		Cl_1	0	−5	−5	10
		Cl_2	40	−26	−26	52
$Cl_5P^{\bullet-}$	C_{4v}	P	2870	−76	−76	152
		Cl_1	0	−1	−1	2
		Cl_2	18	−18	−18	36
$Cl_3P\overset{\bullet}{-}SH_2^+$	C_s	P	1644	−137	−137	274
		Cl_1	0	−17	−17	34
		Cl_2	0	−8	−8	16
		H	0	−8	1	7
$Cl_3PPCl_3^{\bullet+}$	C_{2h}	P	1274	−90	−90	180
		Cl_1	36	−14	−14	28
		Cl_2	3	−6	−6	12
	$C_{2v}{}^b$	P_1	2082	−210	−42	252
		Cl_1	47	−58	−57	115
	$C_s{}^b$	P_1	1617	−211	−211	422
		Cl_1	19	−6	−4	10
		Cl_2	14	−30	−25	55
		Cl_3	11	−27	−22	49
$Cl_3P(SH_2)_2^{\bullet+}$	$C_{2v}(1)^b$	P	2694	−193	−19	212
	$C_2{}^b$	P	2406	−191	−18	209
	$C_{2v}(2)^b$	P	2393	−191	−23	214
	$C_s{}^b$	P	1870	−196	−191	387

[a] Conversion factors from au to MHz: ^{31}P, $A_{iso}(MHz) = 1810A_{iso}(au)$ and $A_{dip}(MHz) = 215A_{dip}(au)$; ^{35}Cl, $A_{iso}(MHz) = 437A_{iso}(au)$ and $A_{dip} = 52A_{dip}(au)$; ^1H, $A_{iso}(MHz) = 4467\ A_{iso}(au)$ and $A_{dip}(MHz) = 531A_{dip}(au)$. [b] UHF wave function.

---

(18) Frisch, M. J.; Head-Gordon, M.; Schlegel, H. N.; Raghavachari, R.; Binkley, J. S.; Gonzalez, C.; DeFrees, D. J.; Fox, D. J.; Whiteside, R. A.; Seeger, R.; Melius, C. F.; Baker, J.; Martin, R. L.; Kahn, L. R.; Stewart, J. J. P.; Fluder, E. M.; Topiol, S.; Pople, J. A. *Gaussian 88*; Gaussian, Inc.: Pittsburgh, PA, 1988. Calculations were performed on an Alliant FX/8 computer at our university.

(19) Dupuis, M.; Spangler, D.; Wendoloski, J. J. *NRCC Program QG01*; Lawrence Berkely Laboratory, Berkeley, 1980. Guest, M. F.; Kendrick, J. *GAMESS User Manual*; Daresbury Laboratory: Daresbury, 1986. Guest, M. F.; Harrison, F. J.; van Lenthe, J. H.; van Corler, L. C. H. *Theor. Chim. Acta* **1987**, *71*, 117. Radial coefficients: P = 0.55, S = 0.65, and Cl = 0.75. Calculations were performed on a Convex C120 computer at the CAOS/CAMM center in Nijmegen.

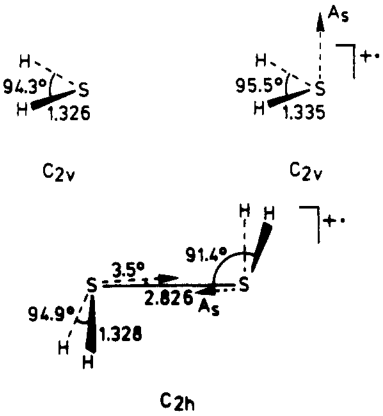

Figure 7. Optimized geometries of the H_2S, $H_2S^{\bullet+}$, and $H_2S\dot{-}SH_2^+$ structures calculated at ROHF/3-21G* SCF level within their respective symmetry constraints.

$H_2S^{\bullet+} + H_2S \rightarrow H_2S\dot{-}SH_2^+$. The homodimer radical cation of H_2S has been subject of many high-level quantum chemical studies.[2,20] The two stable minima found are C_{2v} and C_{2h} structures, of which the C_{2h} is the lowest in energy.[2] The structures resulting after geometry optimization within the C_{2v} symmetry constraint for $H_2S^{\bullet+}$ and H_2S, and C_{2h} symmetry constraint for $H_2S\dot{-}SH_2$ are depicted in Figure 7. Characteristic for the dimer σ^* structure is the long $S\dot{-}S$ bond (2.826 Å). Furthermore, the H–S bond directions are nearly perpendicular to the S–S bond. The hydrogen hyperfine couplings calculated at ROHF/3-21G* level for both the monomer and dimer radical cations are listed in Table V. Sharing the odd electron between two sulfide moieties reduces the dipolar hyperfine coupling of the hydrogen atoms by half. Our calculations on the $H_2S\dot{-}SH_2^+$ radical reveal that the direction of the largest principal value of the sulfur dipolar hyperfine interaction (equivalent to the direction of the largest principal value of the ^{33}S tensor) is not perfectly aligned with the S–S bond direction but makes a small angle (3.5°). The SOMO points away from the hydrogen substituents (Figure 7). Such a nonalignment is experimentally detected in the single-crystal ESR study on the $Me_2S\dot{-}SeMe_2^+$ radical cation.[21] The direction of the largest principal value of the ^{77}Se hyperfine tensor, corresponding to the direction of the SOMO on that nucleus, is inclined by 2.5° to the direction of the minimal g tensor component, which is assumed to correspond to the Se–Se linkage.[21]

$Me_2S^{\bullet+} + Me_2S \rightarrow Me_2S\dot{-}SMe_2^+$. Geometry optimization within C_{2v} symmetry constraint for $Me_2S^{\bullet+}$ and Me_2S and within C_{2h} for $Me_2S\dot{-}SMe_2^+$ results in the structures depicted in Figure 8. All structures are true minima, and their total energies are listed in Table IV. Our results are in excellent agreement with the calculations performed by Illies and co-workers for the same systems.[7i] However, in their article they do not state the symmetry constraints used and give little details on the optimized structures (Figure 8).[7i]

The experimental ratio of the β-hydrogen hyperfine couplings of the monomer and dimer radical cations of Me_2S or Me_2Se is approximately 3.[7f-h,22] The calculated hyperfine couplings are listed in Table V. The ratio of the isotropic couplings of the monomer and the C_{2h} dimer amounts to 2.5. Based on MNDO calculations,[22] Williams suggested[7f-h] that the increased ratio (>2) is a consequence of the nature of the σ^* orbital, rather than of a change in geometry at the heavy atoms. Our ab initio calculations on the C_{2h} structure of $Me_2S\dot{-}SMe_2^+$, along with the computations performed by Illies and co-workers,[7i] show indeed that the bond angles and bond distances of the heavy atoms do not vary much between the monomer and dimer structures. Interestingly, in the C_{2h} dimer the angles between the S–S bond and the bisectors of the C–S–C bond angles are significantly larger than in $H_2S\dot{-}SH_2^+$ (99.9° vs 91.4°, Figures 7 and 8).

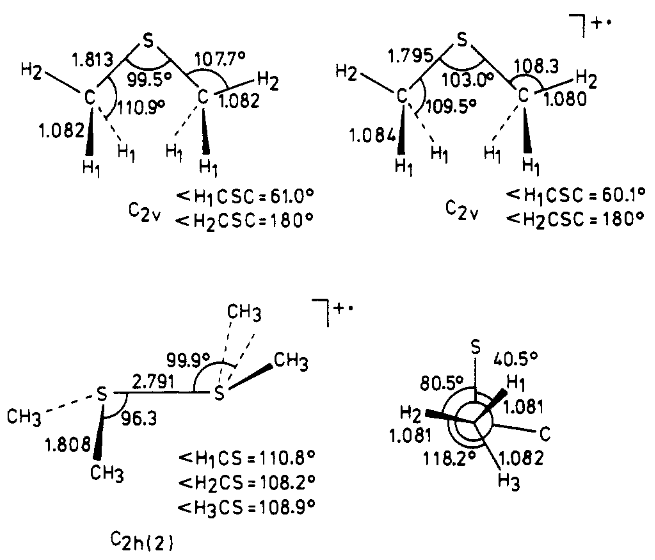

Figure 8. Optimized geometries of the Me_2S, $Me_2S^{\bullet+}$, and $Me_2S\dot{-}SMe_2^+$ structures calculated at ROHF/3-21G* SCF level with their respective symmetry constraints.

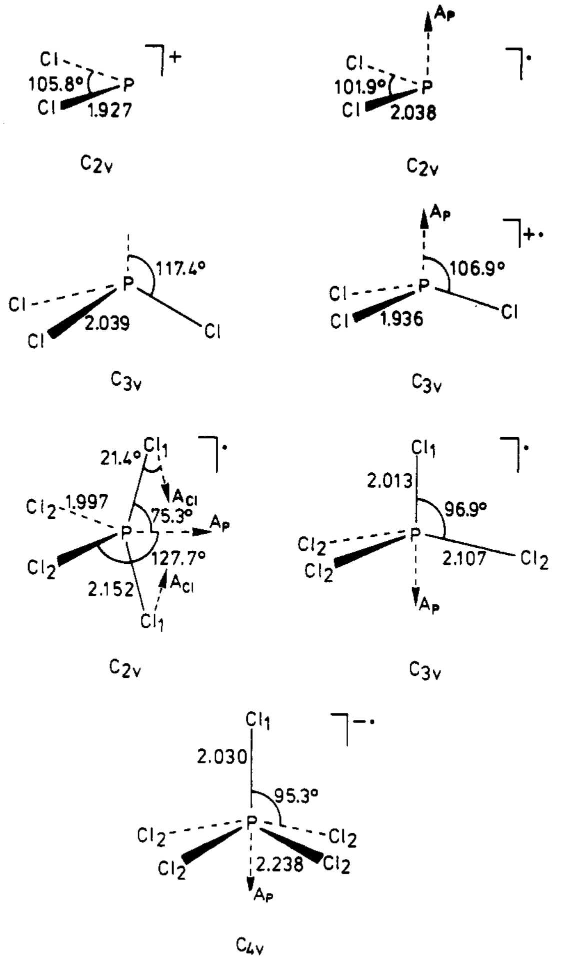

Figure 9. Optimized geometries, calculated at ROHF/3-21G* SCF level, of the structures containing one phosphorus and several chlorine atoms.

The principal direction of the SOMO on the sulfur atoms is almost aligned with the S–S bond. We calculated a small angle of 0.8° in which the orbital points away from the CH_3 substituents. In $H_2S\dot{-}SH_2^+$ the angle of the H–S–H bisector to the SOMO amounts 93.9°, comparable to the 90° of the $3p_z$ orbital in the monomer $H_2S^{\bullet+}$. In $Me_2S\dot{-}SMe_2^+$, however, this angle amounts

---

[20] $H_2S\dot{-}SH_2^+$: (a) Fernandez, P. F.; Ortiz, J. V.; Walters, E. A. *J. Chem. Phys.* **1986**, *84*, 1653. (b) Ortiz, J. V. *Chem. Phys. Lett.* **1987**, *134*, 366. (c) Gill, P. M. W.; Radom, L. *J. Am. Chem. Soc.* **1988**, *110*, 4931.

[21] Nishikida, K.; Williams, F. *Chem. Phys. Lett.* **1975**, *34*, 302.

[22] (a) Glidewell, C. *J. Chem. Soc., Perkin Trans. 2* **1985**, 299. (b) *Ibid.* **1985**, 551.

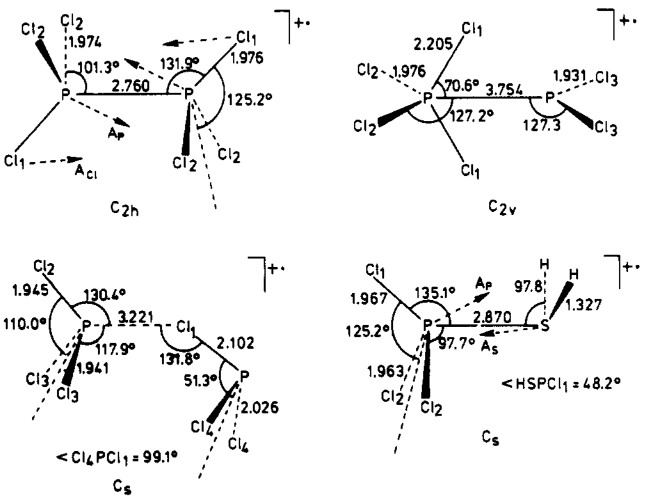

Figure 10. Optimized geometries of the three stationary points found for the $Cl_3P\dot{-}PCl_3^+$ structure (C_{2h} at ROHF, C_{2v} and C_s at UHF) and the heterodimer $Cl_3P\dot{-}SH_2^+$ radical cation (ROHF). Structures calculated with the 3-21G* basis set.

100.7°, which is considerable different. This could have a profound effect on the ratio of the β-hydrogen hyperfine couplings in $Me_2S^{\bullet+}$ and $Me_2S\dot{-}SMe_2^+$.

$Cl_3P^{\bullet+} + Cl_3P \rightarrow Cl_3P\dot{-}PCl_3^+$. Vibrational analysis shows that the C_{3v} structure of the $Cl_3P^{\bullet+}$ cation is a true minimum. Radical formation shortens the P–Cl bonds, with respect to its C_{3v} precursor Cl_3P, by about 0.2 Å. A flattening of the tetrahedral structure is also noted (Figure 9). The calculated C_{2h} structure for $Cl_3P\dot{-}PCl_3^+$ is a true minimum, and the optimized geometry is again characterized by a long σ^* bond (2.760 Å, Figure 10). Formation of the homodimer results in a stabilization of 9.0 kcal/mol at the UHF level (7.1 kcal/mol at ROHF, Table IV), which is almost half of the stabilization calculated for $H_3P\dot{-}PH_3^+$ at different levels (e.g. C_2 = 19.3 kcal/mol at UHF/6-31G*).[2c,d]

The calculated hyperfine couplings of $Cl_3P^{\bullet+}$ and $Cl_3P\dot{-}PCl_3^+$ are enumerated in Table V. The direction of the largest principal value of the ^{35}Cl tensor in $Cl_3P^{\bullet+}$ is inclined by 29.2° with respect to the largest ^{31}P hyperfine tensor component. In the dimer C_{2h} structure, the Cl_1 atoms in the mirror plane (Figure 10) bear a larger spin density than the Cl_2 atoms. The direction of the maximal principal value of the ^{31}P hyperfine tensor is situated between the P–P and P–Cl_1 bonds, inclined by 24.9° to the P–P bond. A similar orientation was established in single-crystal ESR work on related σ^* radical anions of substituted diphosphine disulfides. Experiment and ab initio calculations revealed an angle of 25 to 30°.[23]

$Cl_3P + H_2S^{\bullet+} \rightarrow Cl_3P\dot{-}SH_2^+ \leftarrow Cl_3P^{\bullet+} + H_2S$. As a model for $Cl_3P\dot{-}SMe_2^+$ we optimized the $Cl_3P\dot{-}SH_2^+$ structure. The heterodimer radical cation $Cl_3P\dot{-}SH_2^+$ can be formed following the two different pathways indicated in the heading. The energetics have been envisaged and resulted for respectively the left or right side of the reaction in −16.5 and −15.0 kcal/mol, respectively (Table IV). The C_s staggered structure is computed to be a true minimum (see Figure 10), analogous to the $H_3P\dot{-}SH_2^+$ staggered C_s structure.[2c,d] The stabilization is similar to or even slightly enhanced with respect to the latter one, depending on the theoretical level.

The calculated hyperfine couplings of the $Cl_3P\dot{-}SH_2^+$ radical are listed in Table V. In the C_s structure, atoms in the mirror plane contain the highest spin density. The elongation of the $P\dot{-}S$ σ^* bond is in accordance with its antibonding character. The directions of the SOMO contributions of phosphorus and sulfur are not aligned with the P–S bond direction. The orientation of the anisotropic phosphorus and sulfur contributions to the SOMO (respectively 27.8° and 5.0°, Figure 10) are similar to the angular deviation noted earlier for their respective homodimers $Cl_3P\dot{-}PCl_3^+$ and $H_2S\dot{-}SH_2^+$ (vide supra).

TBP-e $Cl_4P^\bullet$. Geometry optimization within C_{2v} symmetry constraint results in a true minimum for $Cl_4P^\bullet$ (TBP-e, Figure 9). The hyperfine interactions are listed in Table V. In the TBP-e structure major spin density is primarily located on the axial chlorine atoms and the central phosphorus atom. In $Cl_4P^\bullet$ phosphorus is formally hypervalent, and consequently the bonds to the axial chorine atoms are elongated (Figure 9). Analogous to previous calculations on C_{2v} $H_4P^\bullet$ and $F_4P^\bullet$ [16] structures, the Cl_1–P–Cl_1 bond angle in the C_{2v} structure is less than 180°. The direction of the largest principal value of the axial chlorine atoms is inclined to the P–Cl_1 bond direction by 21.4° and nearly orthogonal to the largest ^{31}P hyperfine interaction (83.2°, Figure 9).

Attempts To Calculate the Structure "X". Based on the experimental hyperfine coupling, the structure of the unassigned radical "X" seems similar to the TBP-e $Cl_4P^\bullet$ structure. Geometry optimization of $Cl_4P^\bullet$ within C_{3v} symmetry constraint results in a stationary point (TBP-a, Figure 9). Unfortunately, vibrational analysis shows that it possesses a degenerate imaginary vibrational mode (118*i* cm^{-1}, E). The small value of the force constant of the imaginary mode encountered indicates that the local hypersurface along the direction of this vibrational mode is quite flat. Attempts to minimize the energy of a $Cl_4P^\bullet$ structure within C_s symmetry constraint or without symmetry (C_1) result in dissociation into Cl_3P and a $Cl^\bullet$ atom. Similarly, attempts to optimize the C_{3v} σ^* $Cl_3P\dot{-}Cl$ structure lead to such a dissociation. For the alternative conformation within C_{3v} symmetry, the TBP-a structure, maximal spin density is located at the equatorial chlorine atoms and the central phosphorus atom. The calculated ^{31}P hyperfine coupling is larger than the interaction calculated for the C_{2v} structure (Table V). This is in accordance with previous calculations[16] and could possibly explain the experimental value of "X".

Since both TBP-e $Cl_4P^\bullet$ and "X" radicals are formed on annealing by a rearrangement of the homodimer $Cl_3P\dot{-}PCl_3^+$ cation, we calculated several isomeric structures of $Cl_3P\dot{-}PCl_3^+$ by rearranging a chlorine atom from one phosphorus atom to the other. Only two stationary points were found, and their optimized geometries are depicted in Figure 10.

The first is a C_{2v} structure, composed of a TBP-e $Cl_4P^\bullet$ molecular fragment and a Cl_2P^+ residue. No vibrational analysis could be performed because of computer limitations. The P$\cdots$P distance of 3.75 Å clearly shows that the molecular fragments are loosely bound. The total energy of the C_{2v} structure has increased by 44.3 kcal/mol relative to optimized C_{2h} $Cl_3P\dot{-}PCl_3^+$.

The second stationary point found has been optimized within the C_s symmetry constraint. The resulting structure is composed of two Cl_3P fragments (Figure 10) and represents an intermediate prior to dissociation into a $Cl_3P^{\bullet+}$ radical and a Cl_3P molecule. Although the molecules are 3.22 Å apart, there is still mutual influence on the spin-density distribution. The chlorine atom of the Cl_3P molecule bears some spin density and likewise, the spin density on the central phosphorus atom of the $Cl_3P^{\bullet+}$ radical cation is increased. The total energy lies 6 kcal/mol below the sum of the total energies of the respective C_{3v} $Cl_3P^{\bullet+}$ and Cl_3P structures (Table IV).

Attempts to compute other stable geometries within C_s symmetry constraint failed because of SCF-convergence problems.

$Cl_3P + H_2S\dot{-}SH_2^+ \rightarrow Cl_3P(SH_2)_2^{\bullet+}$. As model compound for $Cl_3P(SMe_2)_2^{\bullet+}$ the structure of the $Cl_3P(SH_2)_2^{\bullet+}$ radical cation was optimized. Geometry optimization of the heterotrimer $Cl_3P(SH_2)_2^{\bullet+}$ resulted in four stationary points (Figure 11, Table IV). We performed vibrational analyses on the $C_{2v}(1)$ and C_s structures. Both resulted in two small imaginary frequencies, indicating no true minima ($C_{2v}(1)$, 92*i* cm^{-1} B_2, 52*i* cm^{-1} B_1; C_s, 89*i* cm^{-1} and 29*i* cm^{-1} A″). The small size of the negative eigenvalues again indicates that the hypersurface for the corresponding vibrational modes is flat.

---

[23] (a) Janssen, R. A. J.; Sonnemans, M. H. W.; Buck, H. M. *J. Chem. Phys.* **1986**, *84*, 3694. (b) Janssen, R. A. J.; van der Woerd, M. J.; Aagaard, O. M.; Buck, H. M. *J. Am. Chem. Soc.* **1988**, *110*, 6001. (c) Aagaard, O. M.; Janssen, R. A. J.; de Waal, B. F. M.; Kanters, J. A.; Schouten, A.; Buck, H. M. *J. Am. Chem. Soc.* **1990**, *112*, 5432.

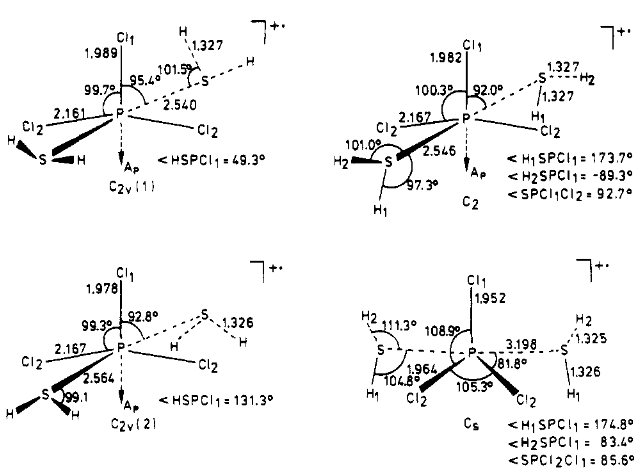

Figure 11. Optimized geometries of the four stationary points found for the $Cl_3P(SH_2)_2^{\bullet+}$ structure. All structures calculated at the UHF/3-21G* SCF level.

The experimental $Cl_3P(SMe_2)_2^{\bullet+}$ radical structure is analogous to the $Cl_5P^{\bullet-}$ radical anion. In order to provide a comparison, we computed the structure of the $Cl_5P^{\bullet-}$ radical anion. Geometry optimization within C_{4v} symmetry constraint gives a true minimum (Figure 9, Table IV). The spin density is located at the equatorial chlorine atoms and the phosphorus atom, similar to the C_{4v} $F_5P^{\bullet-}$ radical anion[16c] and C_{3v} $Cl_4P^{\bullet}$ radical. Therefore, the P–Cl_2 bonds are longer than the P–Cl_1 bond. The SOMO on phosphorus points away from the P–Cl_1 bond. The calculated hyperfine couplings are listed in Table V.

The calculated $Cl_3P(SH_2)_2^{\bullet+}$ radical structures are indeed reminiscent of the $Cl_5P^{\bullet-}$ radical anion (Figure 11) with exception of the C_s structure. In the latter the P–S bond length of 3.16 Å indicates an intermediate structure prior to dissociation into $Cl_3P^{\bullet+}$ and $2H_2S$. Likewise, the calculated ^{31}P hyperfine coupling deviates seriously from the experimental value. The other three structures ($C_{2v}(1)$, $C_{2v}(2)$, and C_2) result in large ^{31}P hyperfine couplings as also found experimentally. However, they are not larger than the hyperfine interaction calculated for $Cl_5P^{\bullet-}$. The total energies are relatively high. In fact, the formation of the $C_{2v}(1)$ structure, by combining a Cl_3P molecule with the $H_2S\dot{-}SH_2^+$ radical cation, is disfavored by 23.4 kcal/mol at the UHF level (23.7 kcal/mol ROHF, Table IV). It should be taken into account that the simplification made by taking H_2S instead of Me_2S as substituent does rule out the possible stabilization via hyperconjugation by the β-hydrogen atoms.

Discussion

It has been shown that X irradiation at low temperature of mixtures of Me_2S and Cl_3P leads to several ion–molecule adducts. The adducts are detected and identified by ESR spectroscopy. In addition, ab initio quantum chemical calculations were performed to provide further insight into the radical structures.

The radiogenic production of the $Cl_3P^{\bullet+}$ radical cation from Cl_3P is straightforward. Analogous to trialkylphosphine radical cations,[4,6] $Cl_3P^{\bullet+}$ reacts with its precursor to yield the homodimeric $Cl_3P\dot{-}PCl_3^+$ radical cation. Likewise for Me_2S, we observe the well-known monopositive cation $Me_2S^{\bullet+}$ and the corresponding homodimer $Me_2S\dot{-}SMe_2^+$. In mixtures of Cl_3P and Me_2S the heterodimer $Cl_3P\dot{-}SMe_2^+$ radical cation is formed, in spite of a significant difference in ionization potential of the two participating molecular fragments. Its formation indicates that, in frozen solution, ionization potential differences are less important for the stability of σ* bonds. At high solute concentrations we detected an ion–molecule reaction between the homodimer $Me_2S\dot{-}SMe_2^+$ and a molecule of Cl_3P. The adduct is assigned to a hetero*trimer* $Cl_3P(SMe_2)_2^{\bullet+}$ radical cation in which the central phosphorus atom bears five substituents. The configuration of this radical is reminiscent of the octahedral $Cl_5P^{\bullet-}$ radical anion. The experimental ^{31}P hyperfine coupling of the heterotrimer exceeds the value[15h] of $Cl_5P^{\bullet-}$ (Table III). In addition, two radical structures arise from a rearrangement of the homodimer radical cation $Cl_3P\dot{-}PCl_3^+$. First, the TBP-e $Cl_4P^{\bullet}$ radical can clearly be identified. Secondly, a possibly related radical structure can be observed ("X"). Until now no final assignment is made for "X". Candidates are a C_{3v} (TBP-a) $Cl_4P^{\bullet}$ radical structure and a σ* $Cl_3P\dot{-}Cl$ radical.

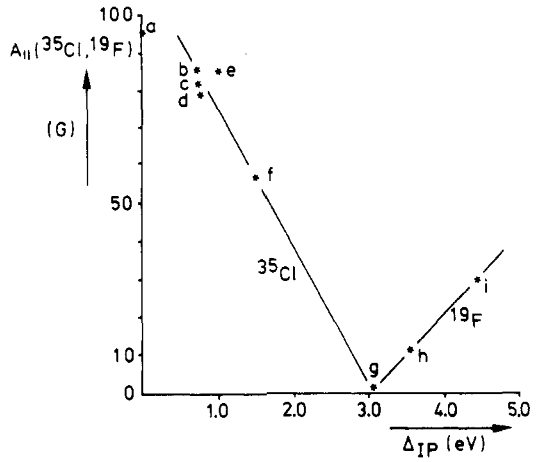

Figure 12. The parallel ^{35}Cl or ^{19}F superhyperfine couplings in σ* ion–$CFCl_3$ adducts as a function of Δ_{IP}. (a) $Cl_2FCCl^{\bullet+}$, ref 1; (b) $EtCl^{\bullet+}$, ref 14b; (c) $(MeO)_2P(H)O^{\bullet+}$, ref 14d. (d) $HCO_2Me^{\bullet+}$, ref 14a; (e) $(MeO)_3P{=}O^{\bullet+}$, ref 14c; (f) $EtBr^{\bullet+}$, ref 14b. (g) $Me_2S^{\bullet+}$, ref 5a, and this study; (h) $Me_2Se^{\bullet+}$, ref 1; (i) $Ph_3P^{\bullet+}$, ref 6e.

Open-shell quantum chemical calculations on the expectation values of the isotropic and dipolar hyperfine coupling constants were performed on the optimized structures of the various monomer and dimer radical structures. The computed values are in general in qualitative agreement with the experimental data and confirm the assignments. Vibrational analyses show that the C_{2h} $Cl_3P\dot{-}PCl_3^+$ homodimer and the C_s heterodimer $Cl_3P\dot{-}SH_2^+$ are true minima. Calculations on the heterotrimer structure did not lead to a true minimum, although vibrational analysis reveals two small imaginary frequencies, indicating that the potential hypersurface for these vibrational modes is flat. It should be emphasized that substitution of Me_2S by H_2S in the calculations affects the electronic distribution within the radical due to the higher ionization potential of H_2S (IP = 10.4 eV). Likewise, it is well known that hyperconjugation of the methyl protons provides significant stabilization for such radical cation complexes despite long central bonds. Moreover, solvent interactions with radical structures can play a decisive role in stabilizing the radical configuration. However, such a stabilization is not yet amenable to computation. Efforts to find a satisfactory $Cl_4P^{\bullet}$ structure for radical "X" did not yield a true minimum. For the C_{3v} (TBP-a) $Cl_4P^{\bullet}$ structure a small degenerate negative eigenvalue is encountered. Geometry optimization of the C_{3v} σ* $Cl_3P\dot{-}Cl$ structure leads to a dissociation of the radical in Cl_3P and $Cl^{\bullet}$.

Interestingly, we find that the extra $CFCl_3$ superhyperfine interactions on $Me_2S^{\bullet+}$ descend from both chlorine and fluorine of the $CFCl_3$ molecule(s). Usually such ion–molecule interaction is observed along the minimal *g* direction,[5a] whereas it now coincides with the maximal *g* direction. Clark[1,2] suggested that the bond strength of a σ* bond depends on Δ_{IP}. Likewise, Clark, Hasegawa, and Symons investigated the change in σ* bond formation from chlorine to fluorine as a function of the difference in ionization potential between $CFCl_3$ and the dissolved molecule.[1] They predict that there should be a certain Δ_{IP} at which interaction switches from chlorine to fluorine. Indeed the $Me_2S^{\bullet+}$ radical cation seems to be this point (Δ_{IP} = 3.18 eV). This is illustrated in Figure 12, where the parallel superhyperfine coupling vs Δ_{IP} is displayed. Two straight lines can be drawn illustrating either superhyperfine interaction to either ^{35}Cl or ^{19}F. However, there seems to be a paradox, since the ^{19}F hyperfine coupling increases with increasing Δ_{IP}, i.e. with decreasing σ* bond strength. Perhaps it is possible to rationalize this discrepancy by assuming a negative sign for the ^{19}F hyperfine coupling. Yet we cannot explain the mechanism involved.

The type of matrix clearly influences radical formation. In the more mobile[7h] matrices, CF_3CCl_3 and $CF_2ClCFCl_2$, the $Me_2S^{\bullet+}$ and $Me_2S{\dot{-}}SMe_2^+$ radicals are observed simultaneously after X irradiation, whereas in the rigid, more crystalline, $CFCl_3$ or CH_2Cl_2 frozen solutions, they are detected separately depending on the concentration. Surprisingly, formation of the $Cl_3P{\dot{-}}PCl_3^+$ homodimer is not observed in the mobile matrices, whereas in spite of ionization potential differences, the $Cl_3P{\dot{-}}SMe_2^+$ heterodimer is readily detected in $CF_2ClCFCl_2$ (but not in CF_3CCl_3!).

The exact mechanism controlling these phenomena is not clear. As a consequence of the absence of $Cl_3P{\dot{-}}PCl_3^+$ radical cation in the mobile matrices, the secondary TBP-e $Cl_4P^{\bullet}$ and "X" radicals are also not detected in these frozen solvents. The experiments show that hyperfine couplings are fairly invariant to the type of freon. In CH_2Cl_2 the coupling for the same radical structure is usually slightly increased. It is noted that by following the reactions in different halocarbon solvents a consistent description of radical formation and reactivity is obtained.

Acknowledgment. This investigation has been supported by the Netherlands Foundation for Chemical Research (SON) with financial aid from the Netherlands Organization for Scientific Research (NWO). Use of the services and facilities of the CAOS/CAMM Center, under grant numbers SON-11-20-700 and STW-NCH-44.0703, is gratefully acknowledged. We thank Mr. Henk Eding for his contributions in the art work.

Registry No. Cl_3P, 7719-12-2; Me_2S, 75-18-3; Cl_3P radical cation (1+), 136889-80-0; Me_2S radical cation (1+), 34480-65-4; Cl_3P dimer radical cation (1+), 136804-95-0; Me_2S dimer radical cation (1+), 76796-56-0; $Cl_3P{\cdot}Me_2S$ radical cation (1+), 136804-91-6; Cl_4P radical, 20762-59-8; $Cl_3P{\cdot}Me_2S{\cdot}Me_2S$ radical cation (1+), 136804-92-7; $Cl_3P{\cdot}H_2S$ radical cation (1+), 136804-93-8; $Cl_3P{\cdot}H_2S{\cdot}H_2S$ radical cation (1+), 136804-94-9; H_2S radical cation (1+), 77544-69-5; H_2S, 7783-06-4; H_2S dimer radical cation (1+), 13604-96-1; Cl_5P, 58765-98-3; Cl_2P^+, 75601-84-2; Cl_2P radical, 20762-58-7.

Electronic Structure and Aromaticity of 1,3-Azaphosphole and 1,3-Azarsole

Tamâs Veszprêmi,*,† Lâszlô Nyulâszi,† Jôzsef Rêffy,† and Joachim Heinicke‡

Department of Inorganic Chemistry, Technical University of Budapest, 1521 Hungary, and Sektion Chemie, Ernst-Moritz-Arndt Universitat, Greifswald, Germany (Received: June 13, 1991)

Three different aspects of the aromaticity have been studied for 1,3-azaphospholes and azarsoles, namely the molecular geometry, the bond separation reactions, and the UV photoelectron spectra. Ab initio molecular orbital theory has been used to calculate the geometrical and electronic structure of the molecules. Comparing the two possible tautomeric forms, the 1*H* derivatives (type I) have planar structures while the 3*H* derivatives (type II) show a puckered structure. The C–P or C–As bond lengths in the type I molecules are definitely shorter and the aromatic stabilization energies calculated from the bond separation reactions are larger than in type II molecules. Within each type I or type II molecules no characteristic difference in the aromaticity could be found. The band structure of the photoelectron spectra of type I molecules is similar to that of pyrrole, and the respective aromatic bands could be recognized.

The large variety of nitrogen-containing heteroaromatic systems inspired chemists dealing with organophosphorus compounds to synthesize heteroaromatic systems containing heavy atoms which replace the nitrogen. The achievements of the synthetic chemists in the 1980s have not been accompanied by widespread theoretical investigations. The photoelectron spectrum of the unstable parent compound phosphaethene[1] has been observed, and numerous quantum-chemical calculations have been conducted on this compound.[2] Among the potentially aromatic metallocycles, phosphabenzene[3] and phosphole[4] have been studied. In our recent work, investigations of 1,3-benzazaphosphole and -benzoxaphosphole have been reported.[5] The photoelectron spectra of methyl-substituted 1,2,4,3-triazaphosphole isomers have been studied, and on the basis of the change of some close-lying states the failure of Koopmans' theorem has been alleged.[6]

In a simple description of the electronic structure of nitrogen-containing heteroaromatic compounds two different types of nitrogen atoms are considered. For the first type the simplest example is pyrrole. The nitrogen atom in pyrrole is substituted by hydrogen that is easily removable by bases possessing acidic character to the parent molecule. In terms of MO theory the aromaticity and stability of pyrrole is the consequence of the interaction of the nitrogen lone pair with the *cis*-butadiene backbone forming a six-electron π-system. For the second type pyridine is the most common example. In this compound nitrogen possesses a basic character. In terms of MO theory this is a consequence of the free lone pair in the plane of the molecule. The aromatic π-sextet can be formally constructed here from the interaction of a C=N double bond and the *cis*-butadiene systems. The least complex compound containing both types of nitrogens is imidazole. According to theoretical investigations the two different nitrogen atoms show similar conjugative ability. The partial charges and the linear coefficients in π-orbitals do not show significant differences between the two different types of nitrogen atoms of imidazole, benzimidazole, and perimidine.[5,7]

When replacing nitrogen by a heavier Group V/a element a diminished interaction is expected due to the small overlap between carbon 2p and phosphorus 3p (or arsenic 4p) orbitals. However, in a recent ab initio study,[8] phosphabenzene was found as 88–90% aromatic as pyridine is, while phosphole is a nonplanar compound in contrast to pyrrole indicating that the aromatic stabilization of the planar state is insufficient to overcome the high inversion

---

† Technical University of Budapest.

‡ Ernst-Moritz-Arndt Universitat.

(1) Lacombe, S.; Gonbeau, D.; Cabioch, J.-L.; Pellerin, B.; Denis, J.-M.; Pfister-Guillouzo, G. *J. Am. Chem. Soc.* **1988**, *110*, 6964.

(2) Gonbeau, D.; Pfister-Guillouzo, G.; Barrans, J. *Can. J. Chem.* **1983**, *61*, 1371. Bruna, P. J.; Krumbach, V.; Peyerimhoff, S. D. *Can. J. Chem.* **1985**, *63*, 1594. Schoeller, W. W. *J. Chem. Soc., Chem. Commun.* **1985**, 334.

(3) Batich, C.; Heilbronner, E.; Hornung, V.; Ashe, A. J.; Clarck, D. T.; Cobley, U. T.; Kilcast, D.; Scanlan, I. *J. Am. Chem. Soc.* **1973**, *95*, 928.

(4) Schafer, W.; Schweig, A.; Mathley, F. *J. Am. Chem. Soc.* **1976**, *98*, 407. Mathey, F. *Chem. Rev.* **1988**, *88*, 429.

(5) Nyulâszi, L.; Csonka, G.; Rêffy, J.; Veszprêmi, T.; Heinicke, J. *J. Organomet. Chem.* **1989**, *373*, 49, 57.

(6) Gonbeau, D.; Pfister-Guillouzo, G.; Barrans, J.; Palmer, M. H. *Chem. Phys.* **1985**, *95*, 243.

(7) Nyulâszi, L.; Pasinszki, T.; Rêffy, J.; Veszprêmi, T.; Thiel, W.; Fabian, J. *Struct. Chem.* **1990**, *1*, 367.

(8) Baldridge, K. K.; Gordon, M. S. *J. Am. Chem. Soc.* **1988**, *110*, 4204.